IEEE Journal of Translational Engineering in Health and Medicine

Received 21 June 2013; revised 18 December 2013; accepted 5 March 2013. Date of publication 26 March 2014; date of current version 9 April 2014.

Digital Object Identifier 10.1109/JTEHM.2014.2313856

Development of a Compact Rectenna for Wireless Powering of a Head-Mountable Deep Brain Stimulation Device

MD KAMAL HOSAIN[1], (Student Member, IEEE), ABBAS Z. KOUZANI[1], (Member, IEEE), SUSANNAH J. TYE[2], OSAMA A. ABULSEOUD[2], ANDREW AMIET[3], AMIR GALEHDAR[3], AKIF KAYNAK[1], AND MICHAEL BERK[1]

[1]School of Engineering, Deakin University, Geelong, VIC 3216, Australia
[2]Department of Psychiatry and Psychology, Mayo Clinic Depression Center, Rochester, MN 55902 USA
[3]Maritime Division, Defence Science and Technology Organisation, Port Melbourne, VIC 3207, Australia

CORRESPONDING AUTHOR: M. K. Hosain (mhosain@deakin.edu.au)

ABSTRACT Design of a rectangular spiral planar inverted-F antenna (PIFA) at 915 MHz for wireless power transmission applications is proposed. The antenna and rectifying circuitry form a rectenna, which can produce dc power from a distant radio frequency energy transmitter. The generated dc power is used to operate a low-power deep brain stimulation pulse generator. The proposed antenna has the dimensions of 10 mm $\times$ 12.5 mm $\times$ 1.5 mm and resonance frequency of 915 MHz with a measured bandwidth of 15 MHz at return loss of -10 dB. A dielectric substrate of FR-4 of $\varepsilon_r = 4.8$ and $\delta = 0.015$ with thickness of 1.5 mm is used for both antenna and rectifier circuit simulation and fabrication because of its availability and low cost. An L-section impedance matching circuit is used between the PIFA and voltage doubler rectifier. The impedance matching circuit also works as a low-pass filter for elimination of higher order harmonics. Maximum dc voltage at the rectenna output is 7.5 V in free space and this rectenna can drive a deep brain stimulation pulse generator at a distance of 30 cm from a radio frequency energy transmitter, which transmits power of 26.77 dBm.

INDEX TERMS Deep brain stimulation, head mountable device, planar inverted-F antenna, passive device, rat, specific absorption rate.

I. INTRODUCTION

Deep brain stimulation (DBS) is an effective therapy for neuropsychiatric disorders, and there is a research need for small, wireless devices [1]. A typical DBS system consists of three major components including an implantable pulse generator (IPG), electrodes, and a programmer. The IPG is the main part of a DBS system. It is a signal generator which is implanted in the subclavicular or chest region of patients. It delivers electrical pulses to the electrodes through an extension lead. The extension lead is an insulated wire that connects the IPG and the electrodes. The electrodes are inserted in the targeted region of the brain to deliver balanced biphasic pulse into the brain. The programmer is used for IPG settings. It communicates with the IPG to set amplitude, frequency, duration, and polarity of the generated signals [2]–[4]. In the existing DBS practices, complications including migration or misplacement of the leads, lead fractures, and skin erosion may happen due to the long extension wires. Battery malfunction and electrode displacement can also cause complications. Moreover, the battery needs to be surgically replaced on a regular basis as it has a limited life span [5]. To reduce the difficulties caused by the battery and the long wires, an antenna can be employed near the electrodes. Wireless transmission and reception of control and power signals can be accomplished with such an antenna [6], [7].

Implantable antennas for different biomedical applications have been investigated in recent years [8], [9]. The size of the implant device will significantly depend on the miniaturization of the antenna. Moreover, maintaining power is a critical issue for long term operation of the implant device. Although the existing IPGs use an antenna for adjusting stimulation parameters wirelessly through the programmer, the IPG is powered by a battery. Sometime dual mode operation (e.g. normal mode, and sleep mode) can improve

the lifetime of the battery [10]. Since this improvement of the battery lifetime is insufficient, research is being carried out to develop alternative techniques including wireless power transmission through rectenna, and inductive coupling [11]. A novel approach of resonance based wireless power delivery over a relatively long distance is presented by RamRakhyani et al. [12]. This implantable coil resonance based system of 22 mm diameter is still too large, thus research on smaller systems is required. Simply a rectifying circuit can be integrated with a miniaturized implantable antenna to form a compact rectenna for wireless power transmission to a DBS pulse generator. Thus, in this paper a rectifying circuit along with a miniaturized antenna as a rectenna is proposed. For practical application of DBS device, it requires laboratory animal testing. Head-mountable DBS devices are popular for animal research, therefore, we proposed our first prototype of a passive device as head-mountable not as implantable. This head-mountable device can be used for a DBS study on rats.

The frequeny of operation for a passive DBS device is also important. Fu-Jhuan et al. [13] reported on a miniaturized implantable planar PIFA at the medical implant communication service (MICS) band of 402 MHz, and the industrial, scientific, and medical (ISM) band of 433 MHz and 2.45 GHz for rectenna application. Gosalia et al. [14] investigated a data telemetry link for retinal prosthesis at microwave frequencies of 1.45 and 2.45 GHz. An intracranial pressure monitoring device implantable in the skull and operating at the 2.4 GHz ISM band was also demonstrated in ref. [15]. We have selected the ISM band of 915 MHz for the DBS antenna because the frequency is higher than the MICS band of 402 MHz, thus offering small antenna size and high data rate. Moreover, the frequency of 915 MHz is lower than the ISM band of 2.4 GHz, therefore, providing less dielectric loss inside biological tissues.

Further progress in DBS depends on the wireless passive device design, and high performance antenna design. The challenge for the antenna design for DBS applications includes making the antenna small in size. In this paper, a compact PIFA with spiral structure is developed. The detail of the designed antenna is discussed in Section II. The paper tackles another challenge that involves designing a small rectifier circuit for RF energy harvesting. However, the first prototype of our passive DBS device is developed for head-mountable application on an animal. In the case of the animal study the DBS device is usually put on the head of animal, thus it is called a head-mountable device. An external energy station transmits power wirelessly as collimated electromagnetic waves to the PIFA. For converting the received RF power to desired DC voltage, a double rectifier is integrated with the antenna. Thus, the antenna, rectifier, and also a low pass filter constitute a rectenna. The paper also presents a miniature DBS pulse generator. The rectenna supplies DC voltage to the DBS pulse generator enabling it to deliver current pulses of desired specification to the target tissue in animal head.

The paper is organized as follows. Section II introduces the theory of the PIFA, feeding techniques, and antenna configuration. Section III describes the performances of the designed PIFA in free space and in vicinity of a six-layer conical rat head model. Section IV describes the wireless power transmission theory followed by the rectenna design, link budget calculation, measurement in free space, and biocompatibility analysis. Measurement result for the passive DBS device powered by the designed rectenna is shown in Section V. Section VI presents discussions. Finally, the concluding remarks are given in Section VII.

II. MINIATURE PIFA DESIGN

A. THEORY OF PIFA

PIFA is generally classified as a monopole antenna although resembling a microstrip antenna. It is a low profile modification of the quarter wave monopole, and belongs to the category of unbalanced antennas. Fig. 1 shows the configuration of a basic PIFA. A PIFA consists of a ground plane, a radiating planar element, a feed wire, and a shorting pin connecting the two planes. The shorting pin establishes a return path for the facial current of the antenna and triggers resonance for electrical dimensions smaller than $\lambda/2$. The shorting pin also helps match the antenna impedance to the feeding/receiving circuit impedance. The PIFA is an attractive antenna for systems where the space volume of the antenna is limited as the antenna size is in the order of $\lambda/4$ [16], [17]. There are no typical equations for designing the PIFA. The resonance frequency (f_r) of the PIFA can be stated as:

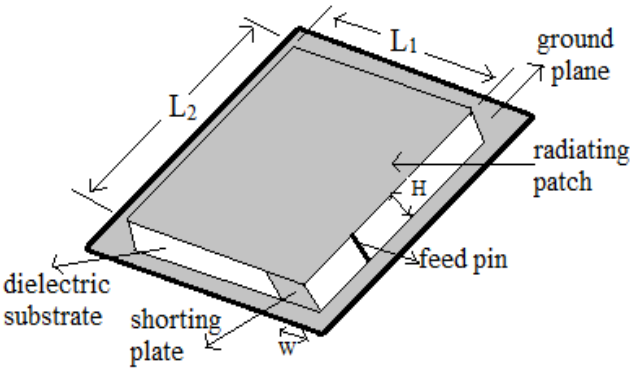

FIGURE 1. The configuration of a simple PIFA.

$$f_r \cong \frac{c}{4(L_1 + L_2 + H - W)} \tag{1}$$

where, c is the speed of light in free space, L_1 and L_2 are the dimension of the radiating element as indicated in Fig. 1, W is the width, and H is the height of the short circuit plate [18]–[21]. The equation (1) does not include the permittivity of the substrate material which significantly influences the resonant frequency of the PIFA [19]. Thus a more comprehensive equation for the resonant frequency of the PIFA is given by [22]:

$$f_r \cong \frac{c}{4\sqrt{\varepsilon_{eff}}(L_1 + L_2 + H - W)} \tag{2}$$

IEEE Journal of Translational Engineering in Health and Medicine

where, ε_{eff} is the effective permittivity of the substrate material between the radiating patch and the ground plane. The effective permittivity ε_{eff} is approximated as [22], [23]:

$$\varepsilon_{eff} \cong \frac{\varepsilon + 1}{2}. \tag{3}$$

Equation (2) can be used to detemine the dimension of the PIFA as shown in Fig. 1. To minimize the overall antenna size (e.g. L_1 and L_2) we used a meandered spiral configuration of radiating element instead of a complete plate as shown in Fig. 2. In our design the total length of the spiral strip line is assigned as the sum of L_1 and L_2.

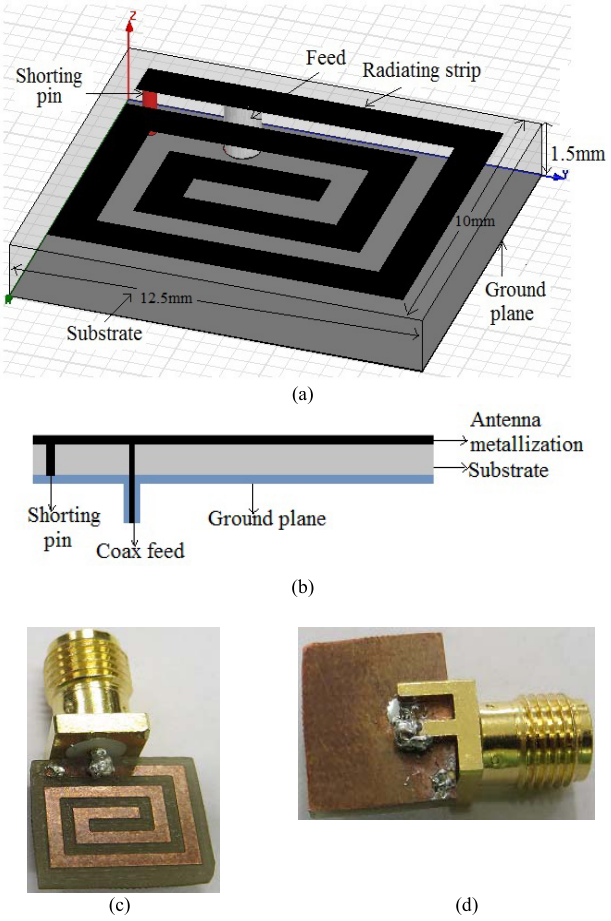

FIGURE 2. (a) Configuration of the proposed PIFA [7]. (b) Geometry of the proposed PIFA. (c) Top view of fabricated antenna. (d) Bottom view of the PIFA.

B. FEEDING TECHNIQUE OF PIFA

Matching is required between the feed line and the antenna to get maximum energy transmission and reception. Matching can be achieved by properly selecting the location of the feed line as the antenna input impedance depends on the location of the feed line in relation to the shorting pin in PIFA. The probe feed method is used in our design. The impedance of the feeding cable is 50 Ω, which is a great compromise between the power handling and the low loss for air dielectric coax. To match this impedance with the antenna input impedance, the central conductor of the coaxial cable must be connected at a certain distance from the shorting pin. To get this feed location, the input impedance of the antenna and the return loss (R_L) are simulated and compared for different positions of the feed point. The optimum feed location is selected based on the value of return loss. The feed location is 5.0 mm away from the edge of the antenna.

On the other hand, the location of the feed point can be derived from the following equations [21]. The wave number (G_1) is written as:

$$G_1 = \frac{W}{120\lambda_0}\left[1 - \frac{1}{12}(k)^2\right]. \tag{4}$$

where, k is the Boltzmann's constant, W is the width of the metallic patch, λ_0 is the free space wavelength at operating frequency. The input impedance is inversely proportional to the wave number. Thus, it can be expressed as:

$$Z_{in} = \frac{1}{G_1}. \tag{5}$$

The distance of the feeding point from the edge of the antenna can be written as:

$$D_{feed} = \cos^{-1}\left(\sqrt{\frac{Z_0}{Z_{in}}}\right) \times \frac{L}{\pi}. \tag{6}$$

where, L is the length of the metallic patch, Z_0 is the impedance of the feed cable, 50 Ω. Equation (6) is used to calculate the position of the feed point for optimum impedance matching. The calculated feed location is 5.09 mm away from the edge of the antenna. Thus a good agreement between the feeding position calculated by this equation and that obtained by the iterative simulation was achieved.

C. ANTENNA CONFIGURATION

Fig. 2(a) presents the configuration of the proposed rectangular spiral PIFA whose dimension is 10 mm × 12.5 mm × 1.5 mm. Fig. 2(b) shows the geometry of the proposed PIFA. The antenna is designed on the dielectric substrate FR-4 of $\varepsilon_r = 4.8$ and $\delta = 0.015$. The FR-4 substrate is used because of its low cost, and availability. The planar inverted-F structure is chosen due to it resonance at $\lambda/4$ length whereas other antennas resonance at $\lambda/2$. Moreover the spiral strip line physically lengthens the current path in two dimensions and hence decline resonance frequency. Thus the spiral PIFA is the best choice for low profile antenna application.

Fig. 2(c) and (d) illustrates the top view and bottom view of the fabricated antenna. The designed antenna was fabricated on a two-layer PCB board with a milling machine. The thickness of copper of 1/2 oz on both side of the substrate makes a two-layer antenna with the total thickness of 1.5 mm. The metallic sheet on the bottom side of the substrate of 10 mm × 12.5 mm dimension works as a ground plane. The rectangular metallic spiral strip on the top of substrate is the radiating element. The overall size of the top radiating metallic strip is 0.8 mm less than the ground plane in each side. The width of the spiral strip line is 1 mm and the distance between

two metallic turns is 0.8 mm. The optimum width of metallic strip and spacing between them is achieved by an iterative method. A shorting pin which minimizes the resonance length of the PIFA of 0.3 mm radius is located at 0.2 mm away from the edge of the strip conductor. A 50 Ω coaxial probe with outer radius of 0.5 mm which is located at 4 mm away from the shorting pin is used to feed the antenna. The SMA connector was attached to the antenna for measuring the input impedance. The proposed design achieves significant miniaturization compared to the previously reported PIFA antennas operating in the UHF band [24], [25].

III. ANTENNA PERFORMANCE

A. IN FREE SPACE

The designed antenna is simulated using finite difference time domain based electromagnetic simulation software XFdtd. As a requirement of the simulation software, free space surrounds the antenna in all sides. The optimal parameters are obtained by an iterative simulation test. The simulated and measured frequency response of the return loss (S_{11}) of the proposed rectangular spiral PIFA in free space is shown in Fig. 3. The bandwidth of 17 MHz (912–929 MHz) including the ISM band of 915 MHz at a return loss of −10 dB was obtained in simulation. The parameter return loss response of S_{11} in free space is also measured with a vector network analyzer. The measurement result reveals that the designed PIFA resonates at the ISM band of 915 MHz and the bandwidth was (912–927 MHz) 15 MHz. Fig. 4 shows the real and imaginary parts of the input impedance versus frequency in free space. It is clear from Fig. 4 that the antenna is capacitive at 915 MHz, though it works as inductive in lower frequency bands. The simulated input impedance of the designed antenna is obtained as Z_i = 45-11.80i Ω at 915 MHz whereas the measured input impedance at 915 MHz is 49.52-18.2i Ω. Thus a significant agreement between the simulated and measured result was achieved.

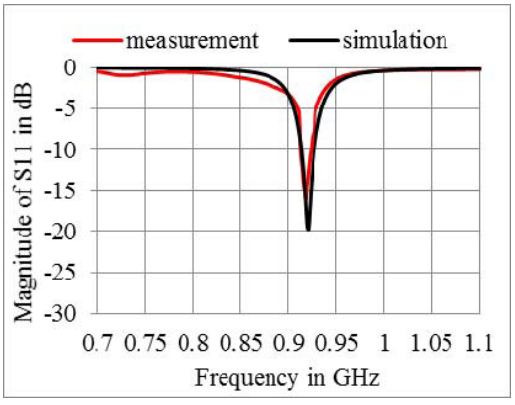

FIGURE 3. Simulated and measured return loss response of the rectangular spiral PIFA in free space.

Fig. 5 demonstrates the 2D far field gain pattern of the proposed antenna in free space. Maximum gain value of

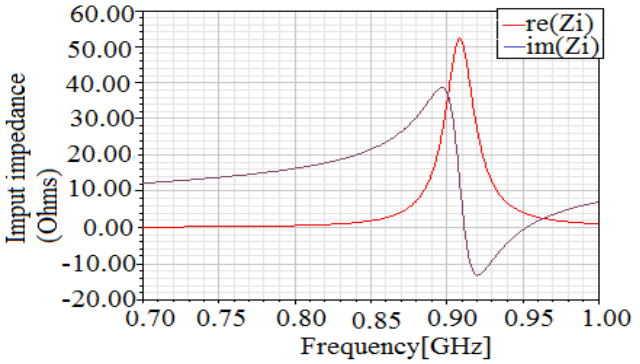

FIGURE 4. Input impedance at the terminal of the antenna.

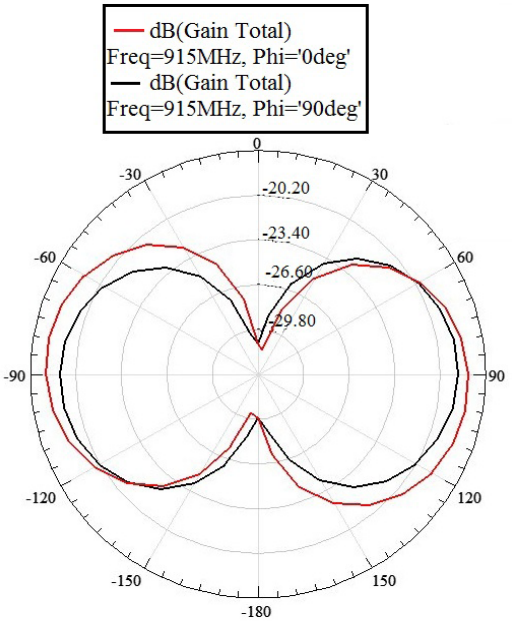

FIGURE 5. Far field 2D gain pattern for the proposed antenna in free space.

−18.08 dB is recorded at $\theta = -80^0$, $\varphi = 0^0$. It is obvious from the radiation patter that the antenna behaves like a top loaded monopole. In order to assess the performances of our designed antenna, we can compare the antenna parameters with those of previously reported antennas. The bandwidth of the designed PIFA of value of 17 MHz is broader than that of 8 MHz for a UHF PIFA reported by Louhichi et al. (2011) [25]. The simulated radiation efficiency of the proposed spiral PIFA is found to be 20.89% at 915 MHz which is higher than the radiation efficiency of 8% presented by Son et al. (2008) [26].

B. WITH A SIX-LAYERS RAT HEAD MODEL

Animal models are extensively used in DBS research to develop new technologies to treat and cure various neurological diseases. Although different animals are used in different research, rats are the most commonly used laboratory animals. DBS research on rats is gaining importance as it can be

IEEE Journal of Translational Engineering in Health and Medicine

modelled for different neurological disease their availability and similarity with human neurons [27]. Moreover, since the antenna has been designed for a head-mountable DBS device, the antenna performance including input impedance and radiation pattern was simulated in vicinity of six-layer rat head model. A six layer rat head was modeled in the simulation software by using dielectric properties of a rat head, and the antenna was placed on it. This head model consists of a cone because the shape of the rat head is generally triangular. Fig. 6 presents the structure of the six-layer head model with the PIFA. For the six-layer conical rat head model, we considered a cone consisting entirely of materials with dielectric property of the rat head tissues. Although the rat head is more complex in structure, here, we considered a simple six-layer conical model to simplify the simulation [28]. The model contains six layers of skin, fat, bone (e.g. skull), dura, cerebrospinal fluid (CSF), and brain. We used a cone of upper radius of 12 mm and lower radius of 7 mm and height of 25 mm as the rat head. The modeled thickness of the skin, fat, skull, dura, and CSF are assumed to be 0.5 mm, 1.0 mm, 1.5 mm, 0.5 mm, and 0.5 mm, respectively. The electromagnetic properties of the materials used in head model at 915 MHz are shown in Table 1.

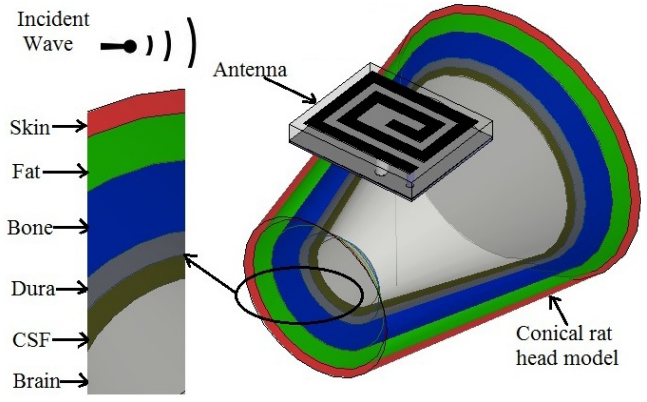

FIGURE 6. Six-layer rat head model and the PIFA.

TABLE 1. Dielectric properties of the rat head model [30]–[32].

Layer Name	Relative Permittivity	Conductivity (s/m)	Mass Density (kg/m^3)
Skin (dry)	40.2	0.8	1080
Fat	15	0.35	920
Bone (skull)	4.9	0.15	1180
Dura mater	44.39	0.966	1030
CSF	68.61	2.419	1010
Brain (Grey matter)	50	1.0	1050

The antenna is subsequently simulated while positioned on the modeled head. The simulation is carried out by a finite difference time domain based EM software XFdtd. In the FDTD simulations, biological tissues and antennas are meshed with cubical FDTD mesh cells of minimum base cell size of $0.5 \times 0.5 \times 0.5$ mm^3. The solution for the minimum grid size of 0.5 mm and target grid size of 0.6 mm is a grid independent solution. Free space padding of twenty times of the base cell, and absorbing boundary in all direction of the model are used during the simulation. The maximum cell step factor used in the simulation is 2. Automatic and sinusoidal sources are used for the broadband and the single frequency simulations, correspondingly. The convergence threshold of -40 dB is settled during the calculation. When the antenna was simulated on the rat head model, the antenna parameters including return loss response (e.g. input impedance) and radiation pattern were changed. The mismatch of the antenna to feed line due to the loading effect of nearby dielectric tissue is mitigated by changing the position of the feeding probe. Moreover, the resonance frequency of the antenna with the rat head model was shifted by 23 MHz towards lower frequency compared with the free space resonance frequency. The 23 MHz shift of resonance frequency is alleviated by reducing the total length of the spiral metallic element. The maximum gain of the antenna attained in the vicinity of the rat head model is -19.11 dB which is 1.0 3 dB lower than the maximum gain in free space. Moreover, the antenna performance with a complete anatomical rat model with thirteen different body dielectrics tissues and a six-layer head model [29] have been analyzed. The results show that the antenna parameters are similar for both the complete anatomical rat model and the six-layer conical rat head model.

IV. WIRELESS POWER TRANSMISSION

A. FIELD'S THEORETICAL DESIGN OF RECTENNA

An accurate evaluation of the DC output power and the conversion efficiency of an RF rectifier require nonlinear circuit analysis. Nonlinear circuit analysis is possible by considering the antenna with an incident EM field as a linear active system which is presented by the Norton equivalent circuit. Let, $J_{eq}(\omega)$ be the Norton equivalent current source, and $Y_A(\omega)$ be the antenna admittance evaluated by the full wave EM analysis. To get $J_{eq}(\omega)$, we have to use the EM theory. An RF source is considered in terms of the associated incident field with certain frequency, direction, and polarization. If the transmitting and receiving antennas are in Fraunhofer regions of each other [33], [34], then the reciprocity theorem can be used to estimate the actual RF power available to the rectifier. The plane wave approximation of the incoming wave is used in this approach to make it simple. Let $E_A(r, \omega)$ be the far field vector radiated by the harvesting antenna in transmitting mode when it is fed by a voltage source of amplitude U and internal resistance R_0. If $E_i(r, \omega)$ is the field vector associated with the incident signal, then by applying the reciprocity theorem, we get:

$$J_{eq}(\omega) = j\frac{[1 + R_0 Y_A(\omega)]}{U}\frac{2\lambda r e^{j\beta r}}{\eta} E_A(r, \omega) \bullet E_i(r, \omega) \quad (7)$$

where, $\bullet$ is the scalar product, Y_A is the antenna admittance, and h is the free space wave impedance. Here, r is the spatial vector indicating the RF source direction of arrival in the

receiver reference frame. The trans-admittance functions can be written as [33]:

$$G_\theta(r,\omega) = j\frac{[1+R_0Y_A(\omega)]}{U}\frac{2\lambda\, r}{\eta}e^{i\beta r}E_{A\theta}(r,\omega) \quad (8a)$$

$$G_\varphi(r,\omega) = j\frac{[1+R_0Y_A(\omega)]}{U}\frac{2\lambda\, r}{\eta}e^{i\beta r}E_{A\varphi}(r,\omega) \quad (8b)$$

Therefore, (7) can be expressed as:

$$J_{eq}(\omega) = G_\theta(r,\omega)\,E_{i\theta}(r,\omega) + G_\varphi(r,\omega)\,E_{i\varphi}(r,\omega) \quad (9)$$

Equation (9) shows the parallel connection of two field-driven current sources with internal admittance $Y_A(\omega)$. The driving fields are the scalar components of the incoming RF signal. The specific direction of the RF wave arrival is described by trans-admittance functions G_φ and G_θ which are derived from the full-wave analysis [33]. Since the current source is linear, the available power of P_{av} at rectenna is simply determined as the power delivered by the antenna under proper impedance match. The available power at rectenna input can be written as [34]:

$$P_{av} = \frac{|J_{eq}(\omega)|^2}{8Re\,[Y_A(\omega)]} \quad (10)$$

The rectenna performance can be determined by the electromagnetic conversion efficiency. The RF-DC conversion efficiency of the rectenna is the parameter that determines the operating range and the output voltage. The conversion efficiency depends on the available microwave input power intensity and the load connected to the diode rectifier. The maximum output voltage and efficiency will be obtained by the optimum input power intensity and load resistance. The RF-DC conversion efficiency also depends on impedance matching between the antenna and the rectifier, and the characteristics of rectifying diode [34]. The RF-DC conversion efficiency can be expressed as:

$$\eta_{RF-DC} = \frac{P_{out}}{P_{av}} \quad (11)$$

where, P_{out} is the DC output power and P_{av} is the available power at rectenna input which is computed by (10). P_{av} can also be determined by the link budget calculation.

B. RECTENNA DESIGN

The schematic diagram of the proposed rectenna is shown in Fig. 7. The rectenna consists of several sections including antenna, matching low pass filter, rectifier, and load resistance. Fig. 8 shows the layout and the fabricated board of the rectenna excluding the antenna. The rectifier circuit, its layout, and return loss response at the input terminal are simulated with Genesys Agilent EM simulating software. The rectifier circuit is fabricated on a PCB board of FR-4 substrate of $\varepsilon_r = 4.8$ and $\delta = 0.015$ with thickness of 1.5 mm. We used SMD circuit elements to minimize the size of our designed rectifier. Fig. 9 illustrates the simulated and measured return loss response of the rectifier circuit with matching low pass filter.

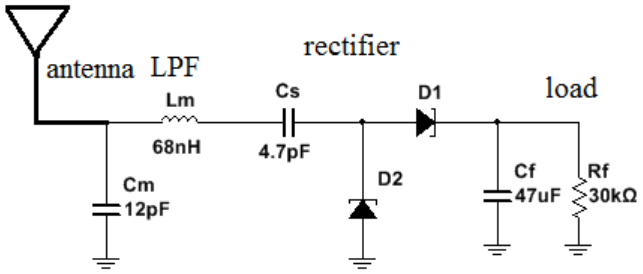

FIGURE 7. Schematic diagram of the designed rectenna.

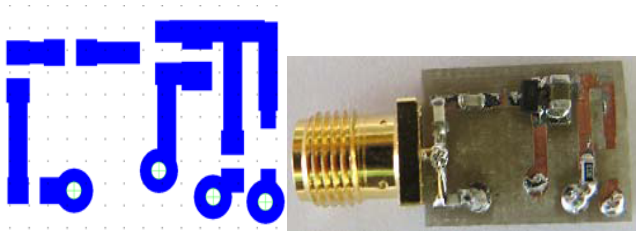

FIGURE 8. Layout and photograph of the fabricated rectifier and the filter circuit.

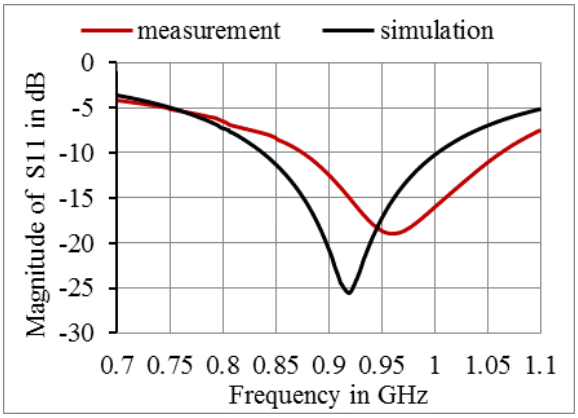

FIGURE 9. Simulated and measured S11 parameters of the rectenna with the low pass filter.

In the rectenna design, a simple L-section impedance matching circuit between the spiral PIFA and the rectifier was used. The L-section circuit consists of a 68 nH inductor and a 12 pF capacitor in the series-parallel configuration as shown in Fig. 7. This L-section circuit matches the antenna impedance of 49.5-18.20i Ω to the rectifier circuit impedance of 3.03-16.808i Ω at 915 MHz. The L-section circuit also works as a low pass filter which passes RF energy at 915 MHz and rejects unwanted higher order harmonics. Thus the harmonics generated by the nonlinear rectifying diode are returned back to it and help generating more DC output power. The simple L-section impedance matching circuit is used to reduce the number of required components of the circuit and thereby minimize the size of the device.

The rectifying circuit for the rectenna consists of couple of Schottky barrier diodes as a rectifying device, a bypass capacitor C_f, a DC blocking capacitor C_s, and a load resistance R_f. The rectifying circuit is a voltage

IEEE Journal of Translational Engineering in Health and Medicine

doubler rectifier. The output rectified voltages of two diodes are added together to offer higher output DC voltage and superior RF to DC conversion efficiency. During the negative cycle of the RF signal, the series capacitor C_s stores charge through the parallel diode. The stored charge is added with the incoming positive cycle of the RF signal for passing through the series diode. Since the rectifying diode plays an impotent role in RF to DC conversion efficiency, we used low forward voltage HSMS-286C Schottky detector diodes. Two diodes are in one package connected in the series-parallel configuration to reduce the size of the device. The equivalent circuit of HSMS-286C comprises of a series resistance R_S = 6 ohms and a zero bias junction capacitance C_{J0} = 0.18 pF. Furthermore the diode characteristics include maximum forward voltage V_F of 350mV, the minimum breakdown voltage V_{br} of 4 V, and high detection sensitivity of up to 50 mV/μW. The capacitor C_f minimizes ripple and passes DC power to the load resistance The more detail operation and performance of some existing rectenna circuit are available in [35]–[37].

C. LINK BUDGET CALCULATION

The passive DBS device requires establishing a secure communication link with the RF energy transmitter. In this link budget setup, the proposed antenna is put on top of the rat head and considered as the receiving antenna. The transmitting antenna is placed at a distant of 25 cm from the receiving antenna. Thus, a communication link is established between the two antennas. To calculate the link budget, it is necessary to know the parameters related to the link. The key parameters are as follows: the operating frequency is 915 MHz, the EIRP of the RF transmitting antenna is 34.77 dBm, and the distance between the transmitting antenna and the receiving antenna is 25 cm. The link budget determines the possibility of wireless power transmission. Table 2 shows the parameters involved in the calculation and the values of the received power P_r [38], [39].

The amount of power received by the receiving antenna (assuming the antennas have a polarization match) is estimated as:

$$P_r = P_t + G_t - L_{tfeed} - L_f - L_a + G_r - L_{Rfeed} \ [dB] \quad (12)$$

TABLE 2. Calculated parameters of the link budget.

Transmitter	
Frequency	915 MHz
Transmitted power (P_t)	26.77 dBm
Transmitter feeding loss (L_{tfeed})	0 dB
Transmitter antenna gain (G_t)	8 dBi
EIRP (P_t+G_t- L_{tfeed})	34.77 dBm
Receiver	
Receiver antenna gain (G_r)	−18.08 dBi
Receiver mismatch loss(L_{Rfeed})	0.11 dB
Propagation	
Distance (d)	25 cm
Free space loss (L_f)	19.6 dB
Air propagation loss (L_a)	0 dB
Received power (P_r)	− 3.04 dBm (0.496592 mW)

where, the free space path loss can be written as:

$$L_f = 10 \ \log_{10}(4\pi \ d/\lambda)^2 [dB]. \quad (13)$$

D. EXPERIMENTAL RESULT OF THE RECTENNA

The collimated wave RF energy transmitter with maximum effective isotropic radiated power (EIRP) of 34.77 dBm was used in our experiment. Since the energy transmitter used in our experiment is fixed, only load resistance is varied to get the optimum output DC voltage. The measured output DC voltage of the proposed rectenna at 915 MHz versus various load resistances in kΩ is shown in Fig. 10 at 25 cm separation. It is clear from Fig. 10 that the output DC voltage increases with increasing the load resistance. The rising rate of the output voltage was higher at lower value of the load resistance than the higher value of the load resistance. The output DC voltage obtained at the load resistance of 7 kΩ is about 57 % of the DC voltage recored at load resistance of 60 kΩ.

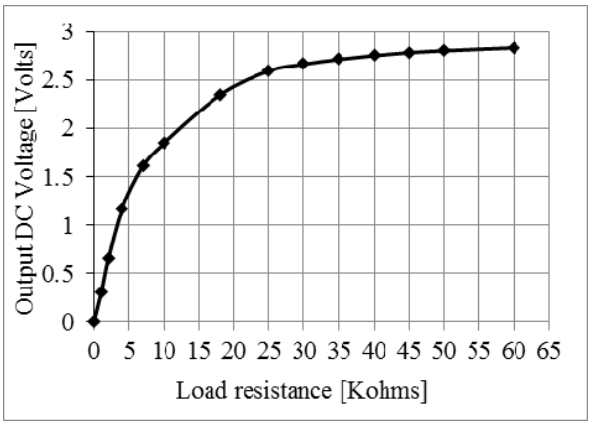

FIGURE 10. Measured output DC voltage of the rectenna versus the load resistance.

Furthermore, with the increment of load resistance the output voltage increases but the current flow through the load, and the RF to DC conversion efficiency declines. The maximum conversion efficiency which is calculated based on (11) is achieved at load resistance of 7 KΩ for the given transmitted power. The RF to DC conversation efficiency of the rectifier at the low input power of −3.04 dBm is 74.56% for 7 KΩ load resistance. It was investigated from the rectifier simulation that the conversion efficiency significantly depends on the transmitted power level. The conversion efficiency will improve if the transmitted power is boosted. Since our designed DBS pulse generator operates at low current level, thus we emphasized on optimization of output voltage. A reasonable output DC voltage with acceptable load current for our application was recorded at the load resistance of 20 kΩ.

The power received by the rectenna hence the out power or DC voltage is also function of separation between the transmitting and the receiving antenna. Fig. 11 shows output DC voltage of the rectenna versus the separation between two antennas for the load resistance of 20 kΩ. The maximum

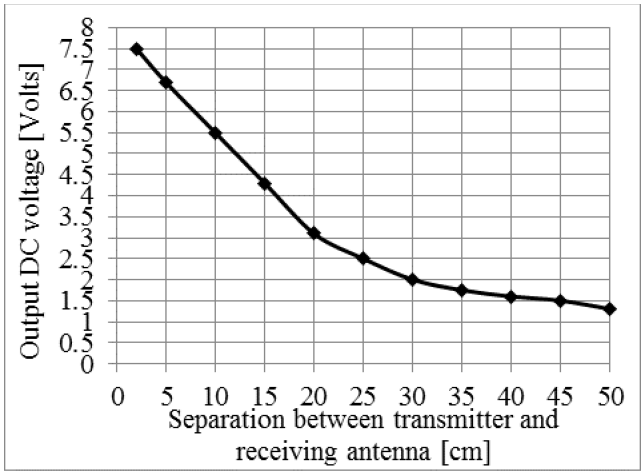

FIGURE 11. Measured output DC voltage of the rectenna versus the distance between transmitter and rectenna.

output DC voltage of 7.5 V was obtained in separation of 2 cm at 20 KΩ load resistance. The output DC voltage decreases with increasing the distance between the two antennas due to the path loss in the air. The required voltage for our designed passive DBS pulse generator of 1.8 V was recorded at separation of 35 cm between the two antennas. The output DC voltage and the operating distance of the DBS device from the energy transmitter can be further increased by improving the antenna gain, the transmitted power, etc.

E. BIOCOMPATIBILITY ANALYSIS

Studies that are intended for the DBS of depressed rats require maintaining the safety regulation of animals. The safety regulation can be verified by the specific absorption rate (SAR) distribution in tissues surrounding the head-mountable passive DBS. Radio frequency electrical current in rectenna will induce electric field in surrounding tissues. Moreover, a part of the radiated EM wave from the far filed transmitter will be directly absorbed into tissues and may increase the tissue temperature. The absorption is due to the power loss with dielectric polarization. The SAR is a measure of the amount of the electromagnetic energy absorbed by biological tissue. The SAR is calculated by measuring the electric field in the stimulated tissue around the device. The formula used for SAR calculation is [21]:

$$SAR = \frac{\sigma}{\rho}|E|^2 = \frac{J^2}{\rho\sigma}[W/kg] \qquad (14)$$

where, E is the rms value of the electric field strength in the tissue [V/m], J is the current density [A/m], σ is the conductivity of body tissue [S/m], and ρ is the density of body tissues [kg/m^3]. The value of SAR depends on the operating frequency, the antenna type and the distance between the antenna and the body tissue. The SAR value increases with increase in the operating frequency because of the penetration depth Also, at higher frequencies the power is absorbed more on the surface.

In order to assess the electromagnetic power absorbed by the surrounding tissues, a numerical analysis of SAR was performed at 915 MHz for the simulation setup shown in Fig. 6 where plane waves are incident on the receiving antenna from a source located at 25 cm distance. According to the link budget calculation in Table 2, the effective radiated power of the incident wave was 34.77 dBm. Fig. 12 shows the rectangular plot of the local and averaged SAR together in the rat head model with the distance from the antenna which is obtained by EM simulation. The calculation method of the local and average SAR is based on the distribution of the electric field as (14). It is obvious from Fig. 12 that SAR is higher near the antenna and then rapidly goes to zero after a short distance. The maximum local SAR value of 0.99 W/kg and the average SAR value of 0.29 W/kg are obtained which are lower than the IEEE C95.1-1999 (1-g average SAR<1.6 W/kg) [40]. Though the international SAR limit may vary depending on national reporting and testing requirement and the network band, the regulation set by American National Standards Institute is generally

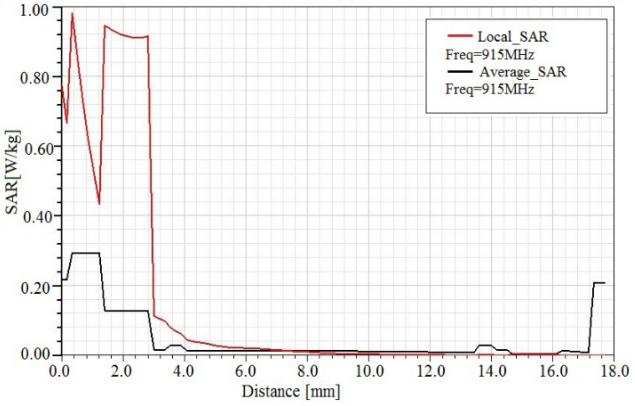

FIGURE 12. Local and average SAR variations at different antenna-head distance.

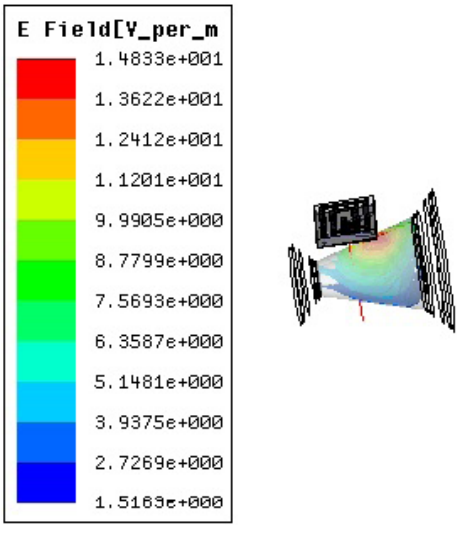

FIGURE 13. Electric field distribution in brain tissue of the rat head model.

followed. So this power harvesting scheme maintain the safety regulation. Fig. 13 illustrates the 3D electric field distribution in the brain of the six-layer rat head model. The value of the maximum electric field in brain tissue is 14.83 V/m. The electric field values in skin, fat, bone, dura, and CSF are 1364 V/m, 1069 V/m, 193 V/m, 27 V/m and 16.3 V/m respectively. The electric field of very low value penetrates the skull and reaches the brain tissues as the antenna is situated outside the head. The electric field in the brain tissue is less than the regulated value as in [41].

V. PASSIVE HEAD-MOUNTABLE DBS DEVICE

Fig. 14 presents the photograph of the prototype passive DBS device. The device comprises three separate PCB boards including antenna, rectifier circuit, and pulse generator circuit [42]. The size of the composite wireless DBS device is approximately 12 mm $\times$ 12 mm $\times$ 4.8 mm. Although, we used three separate boards in our first prototype, the boards could be integrated into a single board. Thus, further size reduction is possible by using multilayer PCB board. The passive DBS pulse generator was operated by the wireless power transmission from an RF energy transmitter. The standard powercast RF transmitter module with effective isotropic radiated power of 34.77 dBm at 915 MHz is used as an RF energy transmitter. The dimension of the powercast energy harvesting transmitter was 17.1 cm $\times$ 15.9 cm $\times$ 4.1 cm. This is a compact transmitter with an integrated antenna of gain of 8 dBi and 60-degree beam pattern. Since the transmitting antenna was not omnidirectional, the passive DBS operated only when receiving antenna was in certain angle of the transmitting antenna.

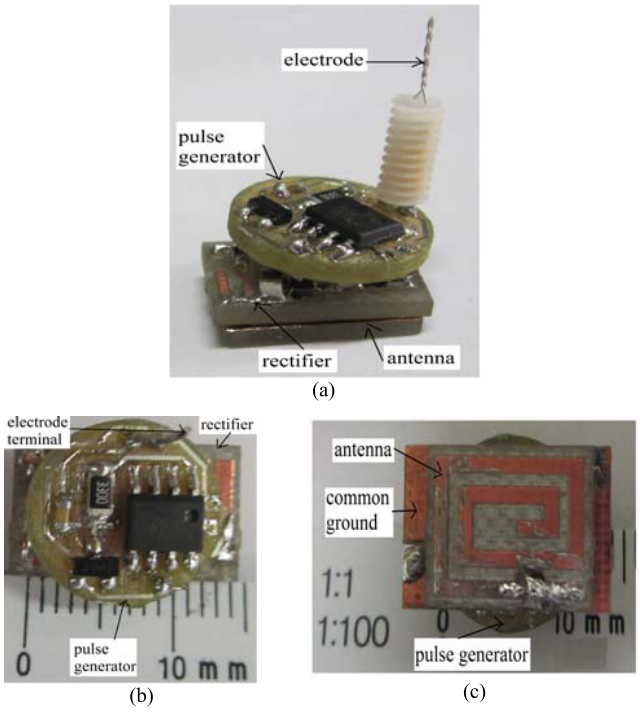

FIGURE 14. **(a) Photograph of the prototype passive DBS device. (b) Top view. (c) Bottom view.**

The experimental setup of the passive DBS pulse generator operating with RF to DC converting rectenna is shown in Fig. 15. The DBS pulse generator successfully generated continuous monophasic current pulses when the maximum separation between the transmitter and the DBS device was 30 cm, the receiving antenna was within 60-degree beam pattern of the RF transmitting antenna, and the receiving antenna's maximum gain direction was towards the transmitter. When the receiving antenna went outside the 60-degree beam direction of the transmitter due to the mobility of rat, the DBS pulse generator was unable to get sufficient power for its operation. However, this problem can be resolved by using a transmitting antenna with an omnidirectional radiation pattern instead of a directional beam pattern.

Further improvement on the operating distance depends on the receiving antenna gain, transmitting power, etc. Though this experiment was performed in free space on the table, it will works in the vicinity of the rat head as it showed almost the same performances when a dielectric material was put underneath the device. The output deep brain stimulating waveform was monitored and measured with a digital storage oscilloscope connected across a 1 kΩ load resistance that modeled the brain tissue [42]. Fig. 16 illustrates the generated wave from our designed passive DBS pulse generator. Based on clinical trials requirements, the duration of the cathodic pulse was set to 90 μs, the frequency of stimulation was set to 130 Hz, and the amplitude of current pulses was set to 200 μA. This passive deep brain stimulating pulse generator is microcontroller based so that the parameters of the stimulating signals can be varied by changing the program of the microcontroller.

VI. DISCUSSION

A compact PIFA was developed and tested. Measurements reveal that the antenna has a bandwidth of 15 MHz at ISM band covering 915 MHz at a return loss of 10 dB. The maximum gain of the PIFA was -18.08 dB. Other promising characteristics of this PIFA include ease of fabrication and impedance matching because the input impedance depends on the position of the feed point with respect to the shorting pin. The antenna had stable characteristics observed by placing different dielectric materials around it. Our designed antenna for rectenna applications was smaller than the antenna designed by Chen et al. [43] and Sun et al. [44]. The gain, efficiency and size could be further improved if the antenna was designed on a low loss ceramic substrate.

The antenna along with the rectifier circuit formed a rectenna. The rectenna consisted of two PCB boards one for the antenna and another for the rectifier circuit. Further size reduction of the rectenna could be achieved by using a multilayer PCB board. Considering the amount of transmitted power, the rectenna supplied the maximum output

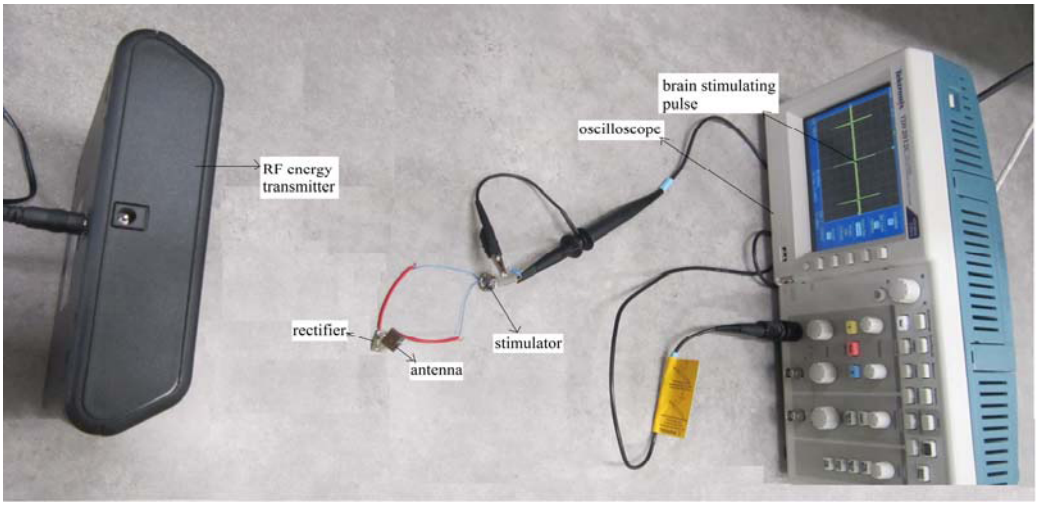

FIGURE 15. Bench top experimental setup for the developed passive DBS device.

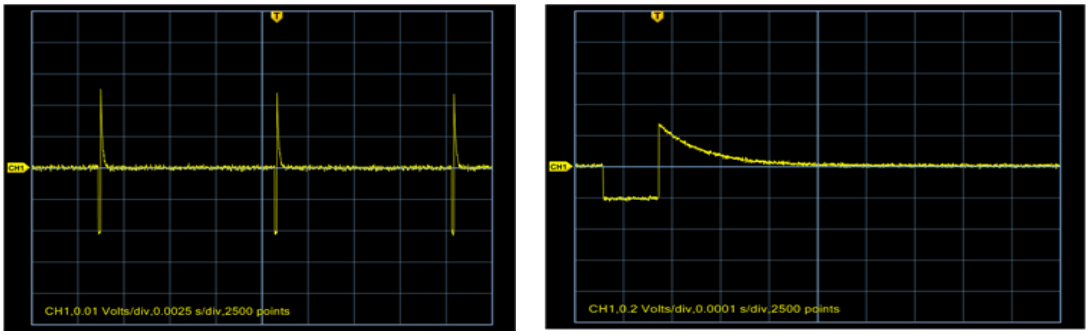

(a) (b)

FIGURE 16. Output waveform of the developed passive DBS device. (b) Close view of the waveform.

voltage of 7.5 V which is higher than the presented voltage by Huang et al. [13]. We used a transmitter of power of less than 26.77 dBm whereas Huang et al. used a 25 W transmitter. To confirm the performance of the proposed rectenna, a DBS pulse generator was operated by it. The rectenna was able to operate the DBS pulse generator successfully at 30 cm distance from the transmitter in free space as well as in vicinity of dielectric substrate. This operating distance is lower than the expected distance according to rectenna performance because the input resistance of the DBS device is higher than the optimum load of the rectenna. Since the passive DBS device was operated in the vicinity of the dielectric substrate, it could be used as a head-mountable DBS device for clinical study of brain stimulation in laboratory animals such as rats. Although the device is designed for DBS studies relating to laboratory rats, it could be easily employed in head-mountable stimulation devices with large animal models including pigs and monkeys. This is because the anatomical structure of larger animals are similar to rats, and the rectenna performance with the biological tissue simulating model is not significantly different from the performance in free space. However, a trivial variation of the antenna can be mitigated easily by changing the length of the metallic strip and the position of the feeding probe. Moreover, to operate this device with an implant in humans or larger animals, a major variation of the design would be necessary due to the significant change of the antenna parameters within this biological environment. Therefore, a comprehensive experimental study will be necessary to make it work with an implant within human body.

The distribution of the electric field and SAR values at 915 MHz were calculated on a rat head model when the rectenna was situated on the head and 34.77 dBm effective power was radiated from an incident wave source at a distance of 25 cm. Although this simple head model gave us some primary indications, it requires a more comprehensive experimental study to validate its practicability. It is obvious from Fig. 12 that the SAR is maximum at around 1.5 mm which was the boundary between the skull and fat. Thus, the skull played an important role in absorption and resistance of the EM waves as very low value of the EM waves penetrated into the brain. It was also observed that some portion of the external electromagnetic field could penetrate into

IEEE Journal of Translational Engineering in Health and Medicine

the brain. Therefore, the SAR distribution must satisfy the regulations set by the American National Standards Institute (ANSI/IEEE).

VII. CONCLUSION

A new rectenna with a spiral PIFA and a double rectifier circuit using schottky barrier diodes has been developed. A miniaturized spiral PIFA was used in this rectenna application because of the space volume limitation of the DBS device. The designed antenna had the measured bandwidth of 15 MHz (912–927 MHz) at a return loss of −10 dB including ISM band of 915 MHz, and the maximum antenna gain of −18.08 dB in free space. The antenna along with the designed rectifier circuit formed a rectenna which provided a maximum DC output voltage of 7.5 V at 2 cm separation between the transmitting and the receiving antenna with a load resistance of 20 kΩ at free space. The rectifier was matched in impedance to the antenna with a L-section matching circuit in between them. The generated DC power was used to drive a passive DBS pulse generator. The experimental result revealed that the developed rectenna successfully operated the DBS device when the RF energy transmitter was 30 cm away from the PIFA. The operating distance could be increased further by enhancing the gain of the rectifier antenna or increasing the power of the RF transmitter.

A great advantage of the rectanna is the fact that it enables the DBS device to operate without a battery. Accordingly, this would help reduce the price of the DBS operation. When used with low-cost head-mountable DBS devices for stimulating laboratory animals, the main price for performing ultra-long term stimulation relates to the battery and its replacement. It is expected that the device will enable saving of around $100 per year when used in low-cost head-mountable DBS devices for laboratory animals. Another advantage of the device is the fact that it enables the head-mountable DBS device to operate indefinitely. The researchers using the device would no longer need to spend their time performing maintenance on the device saving around $500 per year per device. In addition, battery recycling or discarding would not be required enabling saving of around $20 per year per device. In addition, the rectenna can also be used to charge the battery on-board of the implantable stimulation device. Accordingly, if the technology proved effective, it can be considered for use in stimulation devices implanted in human patients having neurological and psychiatric disorders. The technology could benefit thousands of patients having neurological and psychiatric disorders, and also eliminate the requirement of surgery for battery replacement saving millions of dollars each year. We expect that the price of the device, when mass produced, will be less than $5 per device. The entire passive DBS device including energy harvester and pulse generator will cost less than $10. The global annual sale of the device is expected to be in thousands. The sales of this device will increase because of the interest in the use of such device in preclinical research for exploring the treatment of new diseases with the DBS approach.

REFERENCES

[1] R. J. Anderson *et al.*, "Deep brain stimulation for treatment-resistant depression: Efficacy, safety and mechanisms of action," *Neurosci. Biobehavioral Rev.* , vol. 36, no. 8, pp. 1920–33, 2012.

[2] M. A. Liker, D. S. Won, V. Y. Rao, and S. E. Hua, "Deep brain stimulation: An evolving technology," *Proc. IEEE*, vol. 96, no. 7, pp. 1129–1141, Jul. 2008.

[3] C. R. Butson and C. C. McIntyre, "Role of electrode design on the volume of tissue activated during deep brain stimulation," *J. Neural Eng.*, vol. 3, no. 1, p. 1, 2006.

[4] N. Yousif and X. Liu, "Modeling the current distribution across the depth electrode-brain interface in deep brain stimulation," *Expert Rev. Med. Devices*, vol. 4, no. 5, pp. 623–631, 2007.

[5] R. M. Pluta, G. D. Perazza, and R. M. Golub, "Deep brain stimulation," *JAMA: J. Amer. Med. Assoc.*, vol. 305, no. 7, p. 732, Feb. 2011.

[6] S. Santaniello, G. Fiengo, L. Glielmo, and W. M. Grill, "Closed-loop control of deep brain stimulation: A simulation study," *IEEE Trans. Neural Syst. Rehabil. Eng.*, vol. 19, no. 1, pp. 15–24, Feb. 2011.

[7] M. K. Hosain, A. Z. Kouzani, S. Tye, K. Walder, and K. Lingxue, "Design of a miniature UHF PIFA for DBS implants," in *Proc. Presented ICME*, Kobe, Japan, 2012, pp. 485–489.

[8] C. M. Lee, T. C. Yo, C. H. Luo, C. H. Tu, and Y. Z. Juang, "Compact broadband stacked implantable antenna for biotelemetry with medical devices," *Electron. Lett.*, vol. 43, no. 12, pp. 660–662, 2007.

[9] W.-C. Liu, F.-M. Yeh, and M. Ghavami, "Miniaturized implantable broadband antenna for biotelemetry communication," *Microw. Opt. Technol. Lett.*, vol. 50, no. 9, pp. 2407–2409, 2008.

[10] *ZL70101 Medical Implantable RF Transceiver Data Sheet*, Z. Semiconductor, Ottawa, ON, Canada, May 2007.

[11] F. Mounaim and M. Sawan, "Toward a fully integrated neurostimulator with inductive power recovery front-end," *IEEE Trans. Biomed. Circuits Syst.*, vol. 6, no. 4, pp. 309–318, Aug. 2012.

[12] A. K. RamRakhyani, S. Mirabbasi, and C. Mu, "Design and optimization of resonance-based efficient wireless power delivery systems for biomedical implants," *IEEE Trans. Biomed. Circuits Syst.*, vol. 5, no. 1, pp. 48–63, Feb. 2011.

[13] F. J. Huang, C. M. Lee, C. L. Chang, L. K. Chen, T. C. Yo, and C. H. Luo, "Rectenna application of miniaturized implantable antenna design for triple-band biotelemetry communication," *IEEE Trans. Antennas Propag.*, vol. 59, no. 7, pp. 2646–2653, Jul. 2011.

[14] K. Gosalia, G. Lazzi, and M. Humayun, "Investigation of a microwave data telemetry link for a retinal prosthesis," *IEEE Trans. Microw. Theory Tech.*, vol. 52, no. 8, pp. 1925–1933, Aug. 2004.

[15] M. R. Tofighi, U. Kawoos, A. Rosen, and S. Neff, "Wireless intracranial pressure monitoring through scalp at microwave frequencies," *Electron. Lett.*, vol. 42, pp. 148–150, Feb. 2006.

[16] Y. Belhadef and N. Hacene, "PIFAS antennas design for mobile communications," in *Proc. 2011 7th Int. WOSSPA*, Tipaza, Algeria, 2011, pp. 119–122.

[17] K. L. Wong, *Compact and Broadband Microstrip Antennas*, 1st ed. New York, NY, USA: Wiley, Jan. 2002.

[18] T. Taga, "Analysis of planar inverted-F antennas and antenna design for portable radio equipment," in *Analysis, Design and Measurement of Small and Low Profile Antenna*, K. Hirasawa and M. Haneishi, Eds. Boston, MA, USA: Artech House, 1992, ch. 5.

[19] K. L. Wong, *Planar Antennas for Wireless Communications*. New York, NY, USA: Wiley, 2003.

[20] R. Sanchez-Montero, R. Langley, S. Salcedo-Sanz, and J. Portilla-Figueras, "Coplanar hybrid antenna for mobile and wireless applications," *IET Microw. Antennas Propag.*, vol. 5, no. 2, pp. 192–199, 2011.

[21] N. A. Saidatul, A. A. H. Azremi, R. B. Ahmad, P. J. Soh, and F. Malek, "Multiband fractal planar inverted F antenna (F-PIFA) for mobile phone application," *PIER B*, vol. 14, no. 1, pp. 127–148, 2009.

[22] F. Gustrau and D. Manteuffel, *EM Modeling of Antennas and RF Components for Wireless Communication Systems*. New York, NY, USA: Springer-Verlag, 2006.

[23] Y. T. Jean-Charles, V. Ungvichian, and J. A. Barbosa, "Effects of substrate permittivity on planar inverted-F antenna performances," *J. Comput.*, vol. 4, no. 7, pp. 610–614, 2009.

[24] A. Sani, M. Rajab, R. Foster, and Y. Hao, "Antennas and propagation of implanted RFIDs for pervasive healthcare applications," *Proc. IEEE*, vol. 98, no. 9, pp. 1648–1655, Sep. 2010.

[25] O. Louhichi, D. Bechevet, and S. Tedjini, "Methodology for UHF PIFA design in harsh environment," in *Proc. Present. IEEE Int. Symp. Antennas Propag.*, Spokane, WA, USA, Jul. 2011, pp. 1201–1204.
[26] H. Son, W. Choi, and G. Choi, "Radiation efficiency improvement method of RFID tag antenna for metallic objects printed on lossy substrate," in *Proc. APMC*, 2008, pp. 1–4.
[27] T. Karacolak, R. Cooper, and E. Topsakal, "Electrical properties of rat skin and design of implantable antennas for medical wireless telemetry," *IEEE Trans. Antennas Propag.*, vol. 57, no. 9, pp. 2806–2812, Sep. 2009.
[28] L. Yang, D. M. Hao, M. L. Wang, S. C. Wu, and Y. Zeng, "Modeling and simulation of rat head exposed to mobile phone electromagnetic field," *Adv. Res. Compt. Sci. Inf. Eng.*, vol. 153, pp. 422–428, May 2011.
[29] M. K. Hosain and A. Z. Kouzani, "Assessment of functional and biological compatibility of antenna in a head-mountable DBS device using a rat model," *Neurosci. Biomed. Eng.*, vol. 1, no. 1, pp. 73–82, 2013.
[30] C. Gabriel, S. Gabriel, and E. Corthout, "The dielectric properties of biological tissues: I. Literature survey," *Phys. Med. Biol.*, vol. 41, no. 11, p. 2231, 1999.
[31] R. Pethig, "Dielectric properties of body tissues," *Clin. Phys. Physiol. Meas.*, vol. 8, no. 4A, pp. 5–12, 1987.
[32] S. Bri, S. Kassimi, M. Habibi, and A. Mamouni, "Specific absorption rate (SAR) distribution in the human head at global system mobile (GSM) frequencies," *Eur. J. Sci. Res.*, vol. 49, pp. 590–600, Feb. 2011.
[33] D. Masotti and A. Costanzo, "Design of wearable rectennas harvesting from multi-tone ambient RF sources," in *Proc. 4th Int. Symp. Appl. Sci. Biomed. Commun. Tech.*, Catalonia, Spain, 2011, p. 112.
[34] V. Rizzoli, D. Masotti, N. Arbizzani, and A. Costanzo, "CAD procedure for predicting the energy received by wireless scavenging systems in the near- and far-field regions," in *IEEE MTT-S Int. Microw. Symp. Dig.*, May 2010, pp. 1768–1771.
[35] M. Mi, M. H. Mickle, C. Capelli, and H. Swift, "RF energy harvesting with multiple antennas in the same space," *IEEE Antennas Propag. Mag.*, vol. 47, no. 5, pp. 100–106, Oct. 2005.
[36] H. Jabbar, Y. S. Song, and T. T. Jeong, "RF energy harvesting system and circuits for charging of mobile devices," *IEEE Trans. Consum. Electron.*, vol. 56, no. 1, pp. 247–253, Feb. 2010.
[37] J. S. Sun, R. H. Chen, S. K. Liu, and C. F. Yang, "Wireless power transmission with circularly polarized rectenna," *Microw. J. Tech. Library*, 2011.
[38] H. Mizuno, M. Takahashi, K. Saito, N. Haga, and K. Ito, "Design of a helical folded dipole antenna for biomedical implants," in *Proc. 5th EUCAP*, 2011, pp. 3484–3487.
[39] H. Y. Lin, M. Takahashi, K. Saito, and K. Ito, "Development of UHF implanted RFID antenna for medical/health-care applications," in *Proc. XXXth URSI General Assembly Sci. Symp.*, Aug. 2011, pp. 1–4.
[40] *IEEE Standard for Safety Levels with Respect to Human Exposure to Radio Frequency Electromagnetic Fields, 3 kHz to 300 GHz*, IEEE Standard C95.1, 1999.
[41] A. Ahlbom *et al.*, "Guidelines for limiting exposure to time-varying electric, magnetic, and electromagnetic fields (up to 300 GHz)," *Health Phys.*, vol. 74, no. 4, pp. 494–522, 1998.
[42] A. Z. Kouzani, O. A. Abulseoud, S. J. Tye, M. K. Hosain, and M. Berk, "A low power micro deep brain stimulation device for murine preclinical research," *IEEE J. Trans. Eng. Health Med.*, vol. 1, no. 1, pp. 1–9, Jun. 2013.
[43] R. Chen, Y. Lee, and J. Sun, "Design and experiment of a loop rectenna for RFID wirelesspower transmission and data communication applications," in *Proc. PIER*, Beijing, China, 2009, pp. 528–531.

MD KAMAL HOSAIN (S'12) was born in Bangladesh in 1984. He received the B.Sc.Eng. degree from the Khulna University of Engineering and Technology, in 2001. He was a Lecturer with the Department of Electronics and Telecommunication Engineering, Rajshahi University of Engineering and Technology, Bangladesh. He is currently pursuing the Ph.D. degree with Deakin University, Victoria, Australia. His current research interests include development of devices, and antennas and their applications to biomedical engineering, in particular, deep brain stimulation.

ABBAS Z. KOUZANI (M'95) received the B.Sc. degree in computer engineering from the Sharif University of Technology, Tehran, Iran, the M.Eng. degree in electrical and electronics engineering from the University of Adelaide, Adelaide, Australia, and the Ph.D. degree in electrical and electronics engineering from Flinders University, Adelaide, in 1990, 1995, and 1999, respectively. He was a Lecturer with the School of Engineering, Deakin University, Geelong, Australia, and a Senior Lecturer with the School of Electrical Engineering and Computer Science, University of Newcastle, Newcastle, Australia. He is currently an Associate Professor with the School of Engineering, Deakin University. He has been involved in over $2 million research grants, and has published over 240 refereed papers. He served as the Associate Head of School (Research) with the School of Engineering, Deakin University, for several years. He is an OzReader with the Australian Research Council, and reviews for a number of international journals and conferences. He has carried out applied research and consultancy for several Australian and international companies. His current research interests include medical/biological microsystems, microfluidic lab-on-a-chip systems, bioinstrumentation, and biosensors and implants. He is the Leader of Deakin University's BioMEMS Research Group.

SUSANNAH J. TYE received the Ph.D. degree from the Departments of Psychology and Biological Sciences, Macquarie University, in 2008. She received the Post-Doctoral Fellowship with the Department of Neurosurgery, Mayo Clinic, USA. She is currently an Assistant Professor of Psychiatry and Psychology, where she directs the Translational Neuroscience Laboratory, with a focus on developing valid preclinical models of treatment resistant depression and bipolar disorder for investigation of disease and therapeutic mechanisms, utilizing deep brain stimulation. She received a number of grants and awards, including the NCDEU New Investigator Award in 2013, the Mayo/Minnesota Partnership Grant in 2012, the Sir Winston Churchill Fellowship from 2010 to 2011, and the National Alliance for Research on Schizophrenia and Depression Young Investigator Award in 2009. She co-supervises four post-graduate students, two research technicians, and one research fellow. She is a member of the Society for Neuroscience, the Society of Biological Psychiatry, and the International Society of Bipolar Disorder. She has provided a number of community outreach presentations in Australia and the U.S., where she continues to involve with researchers and health psychology professionals to develop school-based mental illness awareness and prevention programs.

OSAMA A. ABULSEOUD received the M.D. degree from Cairo University, Cairo, Egypt, and the M.Sc. degree in general surgery and the Diploma degree in internal medicine from Aim Shams University, Egypt, in 1991, 1996, and 1997, respectively. He received training in General Adult Psychiatry with the University of Southern California, Los Angeles, CA, USA, and a Post-Doctoral Fellowships in mood disorder research with the University of California Los Angeles, a Brain Imaging Research with Huntington Medical Research Institute, CA, USA, and an Addiction Psychiatry with Mayo Clinic. He is a Board Certified in general psychiatry, psychosomatic medicine, and addiction psychiatry. He is an Assistant Professor of Psychiatry with Mayo Medical School, with clinical practice in mood disorders and teaching activities in psychopharmacology. He received a Career Development Award (KL2) to study the effect of nucleus accumbens deep brain stimulation on alcohol consumption in a preclinical model in 2011. He is involved in basic, clinical, and translational research with a focus on studying the disease process and novel therapeutic strategies. He has published 22 papers in peer-reviewed journals. He is a member of the Society of Biological Psychiatry, the International Society of Bipolar Disorder, and the Research Society of Alcoholism.

IEEE Journal of Translational Engineering in Health and Medicine

ANDREW AMIET received the B.Sc.(Hons) degree in physics from Monash University, Melbourne, Australia, in 1990, and started work at the Defence Science and Technology Organisation (DSTO) soon after. He completed the Ph.D. part time degree from Monash University in 2003, developing microwave permittivity and permeability measurement techniques for materials in free space. He is currently the Head of the Electromagnetic Signature Management Group with the Maritime Division, DSTO. His research interests include passive and active radar absorbing material development, and radar cross-section reduction methods.

AMIR GALEHDAR received the B.Eng. degree in telecommunication engineering from K. N. Toosi University of Technology, and the master's (Hons.) and Ph.D. degrees from Griffith University Brisbane, Australia, in 2002, 2005, and 2009, respectively. From 2009 to 2012, he was with the Royal Melbourne Institute of Technology, investigating the electromagnetic behavior of advanced fiber composites and conformal load bearing antenna structure. His research interests are multifunctional platforms, load bearing conformal Carbon-fiber-reinforced polymers antennas, small antennas, and radio frequency identification antennas.

AKIF KAYNAK received the B.Sc. degree from the University of Manchester, Manchester, U.K., the M.Sc. degree from Rutgers University, New Brunswick, NJ, USA, and the Ph.D. degree from the University of Technology, Sydney, Australia. After receiving the Ph.D. degree in 1994, he was an Assistant Professor with the Department of Engineering Sciences, Middle East Technical University, Ankara, Turkey, then as a Research Fellow with the Queensland University of Technology, Kelvin Grove, Australia, before joining the School of Engineering, Deakin University, Waurn Ponds, Australia, in 2001. He is currently an Associate Professor of Mechanical Engineering. Subjects he teaches include Physics, Statics, Dynamics, Stress Analysis, Fibre Science, and Materials Science. His research interests are polymer coatings, functional textiles, and sensors. He is a regular reviewer for various international journals and a co-inventor in a patent on conducting polymer coated wool.

MICHAEL BERK is a NHMRC Senior Principal Research Fellow, and is the Alfred Deakin Chair of Psychiatry with Deakin University, where he heads the IMPACT Strategic Research Centre. He is also an Honorary Professorial Research Fellow with the Department of Psychiatry, the Florey Institute for Neuroscience and Mental Health, and Orygen Youth Health at Melbourne University, as well as with the School of Public Health and Preventive Medicine, Monash University. He is the Past President of the International Society for Bipolar disorders and the Australasian Society or Bipolar and Depressive Disorders. He has published over 500 papers predominantly in mood disorders. His major interests are in the discovery and implementation of novel therapies, and risk factors and prevention of psychiatric disorders. He is the recipient of a number of grants, including the National Institutes of Health, USA, Simon Autism Foundation, NHMRC CRE and project grants, Beyondblue, and Stanley Medical Research Institute awards, and is a Lead Investigator with a Collaborative Research Centre.